Research Article | Vol. 26, No. 16 | 6 Aug 2018 | OPTICS EXPRESS 20920
Optics EXPRESS

Three-dimensional super-resolution high-throughput imaging by structured illumination STED microscopy

YI XUE[1,2] AND PETER T. C. SO[1,2,3,*]

[1]*Dept. of Mechanical Engineering, Massachusetts Institute of Technology 77 Massachusetts Ave., Cambridge, MA 02139, USA*
[2]*Laser Biomedical Research Center, Massachusetts Institute of Technology 77 Massachusetts Ave., Cambridge, MA 02139, USA*
[3]*Dept. of Biological Engineering, Massachusetts Institute of Technology 77 Massachusetts Ave., Cambridge, MA 02139, USA*
[*]*ptso@mit.edu*

Abstract: Stimulated emission depletion (STED) microscopy is able to image fluorescence labeled samples with nanometer scale resolution. STED microscopy is typically a point-scanning method, limited by the high intensity requirement of the depletion beam. With the development of high peak power lasers, two dimensional parallel STED microscopy has been developed. Here, we develop the theoretical basis for extending STED microscopy to three dimensional imaging in parallel. This method uses structured illumination (SI) to generates a three dimensional depletion pattern. Compared to the two dimensional parallel STED microscopy, the 3D SI-STED microscopy generates intensity modulation along the light propagation direction without requiring higher laser power. This method not only achieves axial super-resolution of STED microscopy but also greatly reduces photobleaching and photodamage for 3D volumetric imaging.

OCIS codes: (100.6640) Superresolution; (180.6900) Three-dimensional microscopy; (110.6880) Three-dimensional image acquisition; (180.2520) Fluorescence microscopy.

References and links

1. S. W. Hell and J. Wichmann, "Breaking the diffraction resolution limit by stimulated emission: stimulated-emission-depletion fluorescence microscopy," Opt. Lett. **19**, 780–782 (1994).
2. M. G. Gustafsson, "Surpassing the lateral resolution limit by a factor of two using structured illumination microscopy," J. Microsc. **198**, 82–87 (2000).
3. E. Betzig, G. H. Patterson, R. Sougrat, O. W. Lindwasser, S. Olenych, J. S. Bonifacino, M. W. Davidson, J. Lippincott-Schwartz, and H. F. Hess, "Imaging intracellular fluorescent proteins at nanometer resolution," Science **313**, 1642–1645 (2006).
4. M. J. Rust, M. Bates, and X. Zhuang, "Sub-diffraction-limit imaging by stochastic optical reconstruction microscopy (STORM)," Nature Methods **3**, 793–795 (2006).
5. B. Harke, J. Keller, C. K. Ullal, V. Westphal, A. Schonle, and S. W. Hell, "Resolution scaling in STED microscopy," Opt. Express **16**, 4154–4162 (2008).
6. V. Westphal, S. O. Rizzoli, M. A. Lauterbach, D. Kamin, R. Jahn, and S. W. Hell, "Video-rate far-field optical nanoscopy dissects synaptic vesicle movement," Science **320**, 246–249 (2008).
7. J. Schneider, J. Zahn, M. Maglione, S. J. Sigrist, J. Marquard, J. Chojnacki, H.-G. Krausslich, S. J. Sahl, J. Engelhardt, and S. W. Hell, "Ultrafast, temporally stochastic STED nanoscopy of millisecond dynamics," Nature Methods **12**, 827–830 (2015).
8. P. Bingen, M. Reuss, J. Engelhardt, and S. W. Hell, "Parallelized STED fluorescence nanoscopy," Opt. Express **19**, 23716–23726 (2011).
9. F. Bergermann, L. Alber, S. J. Sahl, J. Engelhardt, and S. W. Hell, "2000-fold parallelized dual-color STED fluorescence nanoscopy," Opt. Express **23**, 211–223 (2015).
10. H. Zhang, M. Zhao, and L. Peng, "Nonlinear structured illumination microscopy by surface plasmon enhanced stimulated emission depletion," Opt. Express **19**, 24783–24794 (2011).
11. A. Chmyrov, J. Keller, T. Grotjohann, M. Ratz, E. d'Este, S. Jakobs, C. Eggeling, and S. W. Hell, "Nanoscopy with more than 100,000 'doughnuts,'" Nature Methods **10**, 737–740 (2013).
12. M. G. L. Gustafsson, "Nonlinear structured-illumination microscopy: wide-field fluorescence imaging with theoretically unlimited resolution," Proc. Natl. Acad. Sci. U. S. A. **102**, 13081–13086 (2005).

#332460 https://doi.org/10.1364/OE.26.020920
Journal © 2018 Received 25 May 2018; revised 9 Jul 2018; accepted 10 Jul 2018; published 31 Jul 2018

Optics EXPRESS

13. M. G. L. Gustafsson, L. Shao, P. M. Carlton, C. J. R. Wang, I. N. Golubovskaya, W. Z. Cande, D. A. Agard, and J. W. Sedat, "Three-dimensional resolution doubling in wide-field fluorescence microscopy by structured illumination," Biophys. J. **94**, 4957–4970 (2008).
14. M. Born and E. Wolf, *Principles of Optics: Electromagnetic Theory of Propagation, Interference and Diffraction of Light* (Elsevier, 2013).
15. M. Gu, *Advanced Optical Imaging Theory* (Springer Science & Business Media, 2000).
16. S. W. Hell, "Toward fluorescence nanoscopy," Nature Biotechnol. **21**, 1347–1355 (2003).
17. P. T. So, H. S. Kwon, and C. Y. Dong, "Resolution enhancement in standing-wave total internal reflection microscopy: a point-spread-function engineering approach," J. Opt. Soc. Am. A Opt. Image Sci. Vis. **18**, 2833–2845 (2001).
18. X. Hao, C. Kuang, T. Wang, and X. Liu, "Effects of polarization on the de-excitation dark focal spot in STED microscopy," J. Opt. **12**, 115707 (2010).
19. Y. Xue, C. Kuang, S. Li, Z. Gu, and X. Liu, "Sharper fluorescent super-resolution spot generated by azimuthally polarized beam in STED microscopy," Opt. Express **20**, 17653–17666 (2012).

1. Introduction

Super-resolution microscopy is able to image fluorescence labeled samples with nanometer scale resolution. The key of super-resolution microscopy is breaking the diffraction limit by different techniques [1–4]. One class of techniques is based on spatial modulation of the excitation beams, including Stimulated Emission Depletion (STED) microscopy [1] and Structure Illumination Microscopy (SIM) [2]. STED microscopy first excites fluorescence molecules in a diffraction limited spot, then applies a donut-shape depletion beam in another wavelength to "turn-off" the fluorescence in the surrounding areas of the excited spot via stimulated depletion. The center area of the excited spot emits fluorescence via spontaneous emission. Typically, STED microscopy is a point-scanning method [1], because of the limited power of lasers for depletion. The higher intensity the depletion beam has, the higher resolution STED microscopy can reach [5]. However, the point-scanning method limits the imaging speed of STED microscopy. The imaging speed is not limited by the scanner speed [6, 7] but by the exposure time per pixel to get a good signal-to-noise ratio (SNR) image. As higher power lasers are available, two dimensional parallel STED microscopy has been realized [8–10] extending on a similar prior work using Reversible Saturable Optical Linear Fluorescence Transitions (RESOFT) mechanism [11]. The donut-shape spot matrix is generated by structured illumination in the parallel 2D STED microscopy [9]. 2D STED microscopy overlaps two incoherent fringe patterns in the orthogonal directions to generate a grid in the focal plane. This grid allows 2D fast imaging of thin samples, however, this approach has no depth sectioning ability for thick samples. The 2D grid pattern cannot deplete the widefield excitation beam in axial direction. At the same time, the 2D grid pattern propagating outside of the focal plane causes photobleaching of samples.

Different from point-scanning STED microscopy, SIM is a widefield super-resolution system that is much faster than point-scanning microscopy [2]. A sinusoidal structured illumination (SI) at spatial frequency k_0 results in generating two copies of the object centered at $\pm k_0$ on the Fourier plane. This displacement allows higher spatial frequencies of the object passing through the objective aperture that acts as a low pass filter. Placing k_0 near the bandwidth limit of the objective can broaden the passband by approximately two [2]. However, the object information from the three copies, at spatial frequencies 0 and $\pm k_0$, are mixed. Unmixing requires taking multiple images with SI at different phases. To achieve even higher resolution, saturated structured illumination microscopy (SSIM) [12] has also been developed. When the excitation intensity is so high that the fluorophore molecules are saturated, the emission pattern becomes nonlinear, which contains higher frequencies components than sinusoidal waves in SIM. However, both SIM and SSIM require complicated image reconstruction process.

Here, we combine the approaches of STED and SIM to enable "simultaneous" three-dimensional super-resolution imaging over a volume. The 3D grid pattern is generated by interference of five coherent beams. In order to achieve comparable performance of the donut-shape beam generated by a vortex phase plate in the point-scanning case, the dark node of the SI should

Optics EXPRESS

satisfy two conditions: (1) the minimum intensity of the dark node is much less than the intensity of the bright node [5]; (2) the shape of the dark node is approximately circular symmetric. The pattern scans in 3D by shifting the relative phases of the five beams on the Fourier plane. This method modulates the out of focus light to form SI along the propagation direction. This modulation increases the axial resolution and reduces the photobleaching at the same time, while keeping the depletion power requirement of 3D SI-STED microscopy the same as that of 2D STED microscopy. In addition, the common path interference design is more robust to external environmental perturbations than the non-common path design.

2. Methods

2.1. Three dimensional structure illumination by five beams interference

Multiple beams interference has been used to generate 3D structured illumination (SI) [13]. However, three beams interference can only generate SI in one radial direction and axial direction rather than all three dimensions [13]. To get symmetric radial super-resolution, the former method rotates the pattern in at least three sequential orientations [13]. Here, we explore coherent interference of five beams, resulting in a 3D grid pattern.

The system diagram is shown in Fig. 1(a). The laser to generate depletion pattern is at 775 nm wavelength. The laser power required for 3D STED is the same as 2D STED assuming minimal sample absorbance. The typically required average power is 2.2 W at 1 MHz repetition rate [9]. The laser beam is collimated by L1 and L2. The collimated beam is diffracted into 5 beams by a diffractive optical element (DOE). In the Fourier plane of the DOE, the phase of each beam is modulated by a spatial light modulator (SLM), which leads to interference pattern shifting in the image plane. The widefield excitation beam is generated by a 635 nm laser diode. A high-NA objective lens (Leica Apo 100x/1.44 Oil) is used in the simulation. To apply SI to STED microscopy, the minimum intensity and the symmetry of the dark node are important. Varying the relative intensity between the center beam and the periphery beams can change the contrast of the interference pattern. When the intensity of the center beam is 2.7 times of the periphery beams, both linear polarization and circular polarization are able to generate dark center ($I_{\min}/I_{\max} < 10^{-5}$), defined as "zero intensity" (Fig. 1(b)).

The diffraction theory shows spatial resolution is proportional to the numerical aperture (NA) of the objective [14]. In super-resolution microscopy, we normally choose a high-NA objective to achieve high resolution. We calculated the five beams coherent interference based on the vector Debye theory [15]. If the five beams are all circular polarized, the electric fields of each beam near the specimen plane are (ignoring the same temporal factor for each beam):

$$\begin{cases} \mathbf{E_1} = A_1(x\hat{x} + iy\hat{y})\exp\left[i(k_z z\hat{z} + \alpha_1))\right] \\ \mathbf{E_2} = A_2(\cos\theta x\hat{x} + iy\hat{y} + \sin\theta z\hat{z})\exp\left[i(k_x \sin\theta x\hat{x} + k_z \cos\theta z\hat{z} + \alpha_2))\right] \\ \mathbf{E_3} = A_3(\cos\theta x\hat{x} + iy\hat{y} - \sin\theta z\hat{z})\exp\left[i(-k_x \sin\theta x\hat{x} + k_z \cos\theta z\hat{z} + \alpha_3))\right] \\ \mathbf{E_4} = A_4(x\hat{x} + i\cos\theta y\hat{y} + i\sin\theta z\hat{z})\exp\left[i(k_y \sin\theta y\hat{y} + k_z \cos\theta z\hat{z} + \alpha_4))\right] \\ \mathbf{E_5} = A_5(x\hat{x} + i\cos\theta y\hat{y} - i\sin\theta z\hat{z})\exp\left[i(-k_y \sin\theta y\hat{y} + k_z \cos\theta z\hat{z} + \alpha_5))\right]. \end{cases} \quad (1)$$

If the five beams are linear polarized at 45° angle to x axis, the electric fields of each beam are:

$$\begin{cases} \mathbf{E_1} = A_1(x\hat{x} + y\hat{y})\exp\left[i(k_z z\hat{z} + \alpha_1))\right] \\ \mathbf{E_2} = A_2(\cos\theta x\hat{x} + y\hat{y} + \sin\theta z\hat{z})\exp\left[i(k_x \sin\theta x\hat{x} + k_z \cos\theta z\hat{z} + \alpha_2))\right] \\ \mathbf{E_3} = A_3(\cos\theta x\hat{x} + y\hat{y} - \sin\theta z\hat{z})\exp\left[i(-k_x \sin\theta x\hat{x} + k_z \cos\theta z\hat{z} + \alpha_3))\right] \\ \mathbf{E_4} = A_4(x\hat{x} + \cos\theta y\hat{y} + \sin\theta z\hat{z})\exp\left[i(k_y \sin\theta y\hat{y} + k_z \cos\theta z\hat{z} + \alpha_4))\right] \\ \mathbf{E_5} = A_5(x\hat{x} + \cos\theta y\hat{y} - \sin\theta z\hat{z})\exp\left[i(-k_y \sin\theta y\hat{y} + k_z \cos\theta z\hat{z} + \alpha_5))\right]. \end{cases} \quad (2)$$

Optics EXPRESS

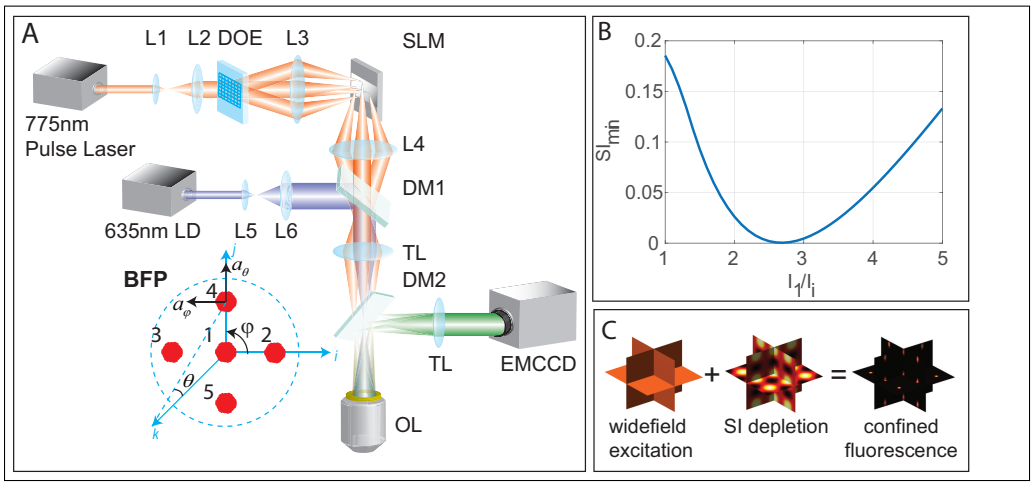

Fig. 1. (A) The diagram of the 3D SI-STED microscopy. The 635 nm excitation beam generates widefield illumination on the image plane. The 775 nm depletion beam generates 3D SI on the image plane by phase modulation on the Fourier plane using spatial light modulator (SLM). (B) The minimum intensity of SI becomes zero (in the center of dark nodes) when the center beam is 2.7 times brighter than the other four beams. (C) The diagram shows confined fluorescence signals are generated after widefield excitation and SI depletion.

In Eq. (1) and Eq. (2), A_i is the amplitude of each beam, (x, y, z) is the coordinate in the image domain, $(\hat{x}, \hat{y}, \hat{z})$ is the unit vector, (k_x, k_y, k_z) is the wave vector, θ is the angle of numerical aperture shown in Fig. 1, α_i is the relative phase of each beam. The sum of these five electric fields is the interference field in the image domain, which is a 3D grid pattern.

The coherent interference pattern of the five beams is described in Eq. (3) that shows the circular polarized case (Eq. (2)). For linear polarized beam, the result is similar but our simulation focuses on circular polarized case in this paper. According to Eq. (3), there are 17 independent Fourier components of the interference pattern:

$$
\begin{aligned}
I =& A_1^2 + A_2^2 + A_3^2 + A_4^2 + A_5^2 \\
&+ A_1A_2 \cos\left[k_x \sin\theta x + k_z(\cos\theta - 1)z + \alpha_2 - \alpha_1\right](\cos\theta + 1) \\
&+ A_1A_3 \cos\left[k_x \sin\theta x - k_z(\cos\theta - 1)z - \alpha_3 + \alpha_1\right](1 - \cos\theta) \\
&+ A_1A_4 \cos\left[k_y \sin\theta y + k_z(\cos\theta - 1)z + \alpha_4 - \alpha_1\right](\cos\theta + 1) \\
&+ A_1A_5 \cos\left[k_y \sin\theta y - k_z(\cos\theta - 1)z - \alpha_5 + \alpha_1\right](1 - \cos\theta) \\
&+ 2A_2A_3 \cos(2k_x \sin\theta x + \alpha_2 - \alpha_3) \sin^2\theta \\
&+ 2A_4A_5 \cos(2k_y \sin\theta y + \alpha_4 - \alpha_5) \sin^2\theta \\
&+ A_2A_4\left[2\cos\theta \cos(k_x \sin\theta x - k_y \sin\theta y + \alpha_2 - \alpha_4)\right] \\
&+ A_2A_4\left[\sin^2\theta \sin(k_x \sin\theta x - k_y \sin\theta y + \alpha_2 - \alpha_4)\right] \\
&- A_3A_5\left[2\cos\theta \cos(k_x \sin\theta x - k_y \sin\theta y + \alpha_5 - \alpha_3)\right] \\
&- A_3A_5\left[\sin^2\theta \sin(k_x \sin\theta x - k_y \sin\theta y + \alpha_5 - \alpha_3)\right] \\
&+ A_2A_5 \sin(k_x \sin\theta x + k_y \sin\theta y + \alpha_2 - \alpha_5) \sin^2\theta \\
&- A_3A_4 \sin(k_x \sin\theta x + k_y \sin\theta y + \alpha_4 - \alpha_3) \sin^2\theta.
\end{aligned}
\tag{3}
$$

Optics EXPRESS

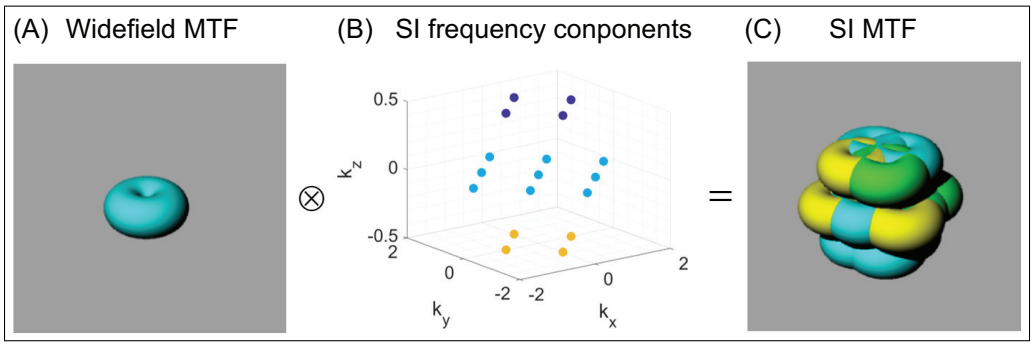

Fig. 2. The coherent interference of five beams fills the "missing cone" of widefield illumination. (A) MTF of widefield illumination that shows the "missing cone" in Fourier domain. (B) Frequency components of five beams coherent interference. Different colors are used for identify different frequency components. (C) MTF of SI that has no "missing cone".

In the Fourier domain, the coherent interference of these five beams generates 17 spatial frequency components (Fig. 2(b)). Without the interference pattern, widefield microscopy has a finite support in k_z of the frequency domain, other than $k_z = 0$ point, the frequency components are zeros [13, 15] (Fig. 2(a)). The interference pattern can fill the "missing cone" by convolution of these two modulation transfer functions (MTF) (Fig. 2(c)). To reconstruct all frequency components, at least 17 independent intermediate images are required for SIM. For SI-STED microscopy, because the efficient excitation pattern is much sharper than sinusoidal pattern, it requires more intermediate images depending on the depletion power (see Results). Each intermediate image is a snapshot of structured illuminated sample with phase shifting $\Delta\alpha_i$ on the Fourier plane, which equivalently shifting the locations of the illumination pattern in image plane. After collecting all intermediate images and reconstructing the image (section 2.3), the reconstructed MTF is the convolution of widefield MTF and SI MTF (Fig. 2). Compared to three beams intereference [13], the five beams interference in our work intrinsically forms symmetric patterns in 3D without any rotation of samples.

2.2. SI-STED depletion process

Previous works of STED microscopy [9] has derived the equations governing fluorescence stimulated depletion process in parallel STED microscopy. The interference angle is the same as numerical aperture angle. We modified the equation to calculate the full width half maximum (FWHM) of the super-resolution spot is:

$$d = \frac{\lambda_{STED}}{2NA} \cdot \frac{1}{\sqrt{4 + (\pi/2)^2 \cdot \frac{I_{max}}{I_{sat}} \cdot \frac{\sin\omega}{\sin\theta}}}, \tag{4}$$

where $I_{\max}$ is the maximum intensity of the standing wave for depletion and I_{sat} is the saturation intensity of the fluorophore. ω is the equivalent interference angle for structured illumination pattern. Increasing $I_{\max}$ leads to higher spatial resolution (Fig. 3).

2.3. Parallel scanning and image reconstruction

To scan the whole field of view (FOV), we shifted the relative phase of the five beams on the Fourier plane. Each phase shifting generates an intermediate image for later reconstruction. For example, shifting the phase of the 2$^{\text{nd}}$ beam by $\Delta\alpha_2 = +\alpha$ and the phase of 3$^{\text{rd}}$ beam by $\Delta\alpha_3 = -\alpha$ moves the illumination pattern in the horizontal direction. Similarly, relative phase shifting of the

Optics EXPRESS

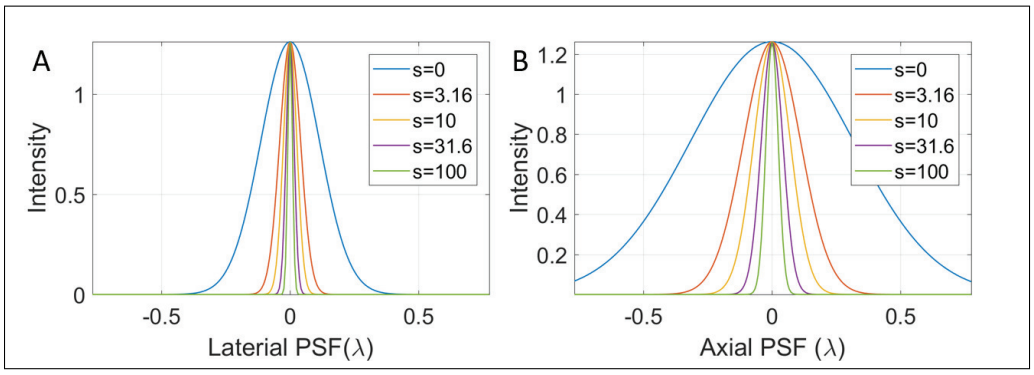

Fig. 3. The PSF of effective emission spot under different depletion power. $s = I_{\max}/I_{\text{sat}}$. The widefield PSF is corresponding to $s = 0$.

4th beam by $\Delta\alpha_4 = +\alpha$ and 5th beam by $\Delta\alpha_5 = -\alpha$ moves the pattern in the vertical direction. Shifting the phase of center beam (1st beam) leads to axial scanning (Fig. 1).

We reconstructed the super-resolution image from the intermediate images. For SIM technique, the illumination pattern can be described as sinusoidal wave with a few orders of Fourier components (say m order). In this case, the number of intermediate images required for reconstruction is $2m + 1$ [17]. This calculation is based on the assumption that the illumination pattern is sinusoidal wave. However, the effective emission region of SI-STED microscopy contains much higher orders of spatial frequency components. The spatial frequency content is not only related to the illumination pattern period but also related to the depletion power. Thus, the number of intermediate images for reconstruction cannot be estimated simply from the pattern period (see Section 3.2 for details). Thus, we decompose the effective emission region of SI-STED microscopy by a series of impulse function rather than sinusoidal waves [17].

The reconstructed image $I'(\mathbf{r})$ can be expressed as a sum of intermediate images recorded at a set of translation shifting vectors $\mathbf{r}'$ modified by the corresponding weighting function $f(\mathbf{r}, \mathbf{r}')$. In each step, we recorded one intermediate image $I(\mathbf{r}, \mathbf{r}')$. The weighting function is an impulse function, that is, $f(\mathbf{r}, \mathbf{r}') = \delta(\mathbf{r} - nT - \mathbf{r}')$, where T is the period of SI in the direction of $\mathbf{r}$. Thus, the reconstructed image is

$$I'(\mathbf{r}) = \sum_{\mathbf{r}'} f(\mathbf{r}, \mathbf{r}')I(\mathbf{r}, \mathbf{r}') = \sum_{\mathbf{r}'} \delta(\mathbf{r} - nT - \mathbf{r}')I(\mathbf{r}, \mathbf{r}'). \tag{5}$$

3. Results

3.1. Structure illumination by different polarized beams

First, we evaluated the dark node intensity and symmetry of the illumination pattern. For a beam with linear polarized angle α, the polarization matrix is $\binom{\cos\alpha}{\sin\alpha}$; for circular polarized beam, the polarization matrix is $\frac{1}{\sqrt{2}}\binom{1}{i}$ (Fig. 4). We normalized the total input power, that is, the sum of the five beams intensity is one. Circular polarized beams are able to generate symmetric interferometric patterns (Fig. 4(b)), whereas the dark area of linear polarized beams interference is asymmetric (Fig. 4(a)). Noticed the curvature of the dark area along the $\pi/4$ diagonal (Fig. 4(a), red dot plot) is much smaller than that along the $3\pi/4$ diagonal. This asymmetry of dark area results in the asymmetry of the depletion effect, furthermore leading to asymmetric super-resolution PSF. Thus, it is significant to have circular polarized beams in SI-STED microscopy. This conclusion is consistent with point-scanning STED microscopy, in which only circular polarized beam and other central symmetric polarized beam can generate symmetric donut-shape

Optics EXPRESS

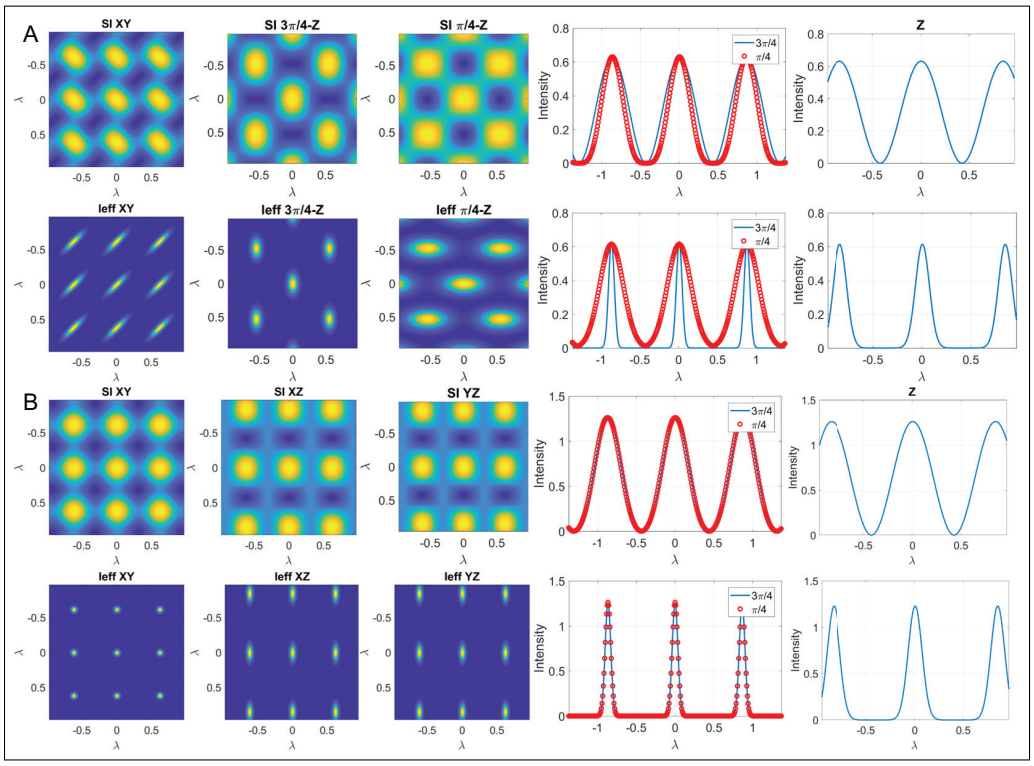

Fig. 4. Depletion patterns and effective emission regions of SI-STED microscopy (I_{max}/I_{sat} = 10) (A) by $\pi/4$ linear polarized beams and (B) by circular polarized beams. Linear polarized beams generate asymmetric depletion pattern, while circular polarized beams generate symmetric depletion pattern. Both cases use uniform widefield illumination as excitation beam.

spot after the vortex phase plate [18, 19].

3.2. SI-STED reconstruction

The reconstruction process follows the algorithm in section 2.3. The comparison of widefield microscopy and SI-STED microscopy after reconstruction shows in Fig. 5. Under our simulation conditions, the lateral resolution of widefield microscopy is 346.7 nm, and the axial resolution is 649.6 nm. After the reconstruction, the SI-STED microscopy reaches 59.9 nm lateral resolution and 163.2 nm axial resolution that are 6-fold and 4-fold narrower than the widefield microscopy respectively. The MTF of SI-STED microscopy is broader correspondingly. For parallel STED microscopy, the depletion energy per dark node is about 1 nJ in the previous work [9], and the period of structured illumination is 374 nm. Thus, the power density of each dark node as depletion beam is about 1.5 MW/cm^2, which is lower than the typical power density used for single point-scanning STED microscopy. The power is limited by the laser total power and the thermal damage threshold of biological sample. Because each bright node in the structured illumination pattern shared by multiple unit cells, paralleled STED microscopy has higher power efficiency than single point-scanning STED microscopy [9]. Each bright node in the 3D structured illumination pattern is shared by 6 unit cells rather than 4 unit cells in the 2D case. Thus, 3D parallel STED microscopy has higher power efficiency than 2D parallel STED microscopy. The lateral period of 3D structured illumination is 473.9 nm (Fig. 4), therefore the power per unit cell is 3.36 mW under the same power density as 2D case. The laser has 2.2 μJ output power

Optics EXPRESS

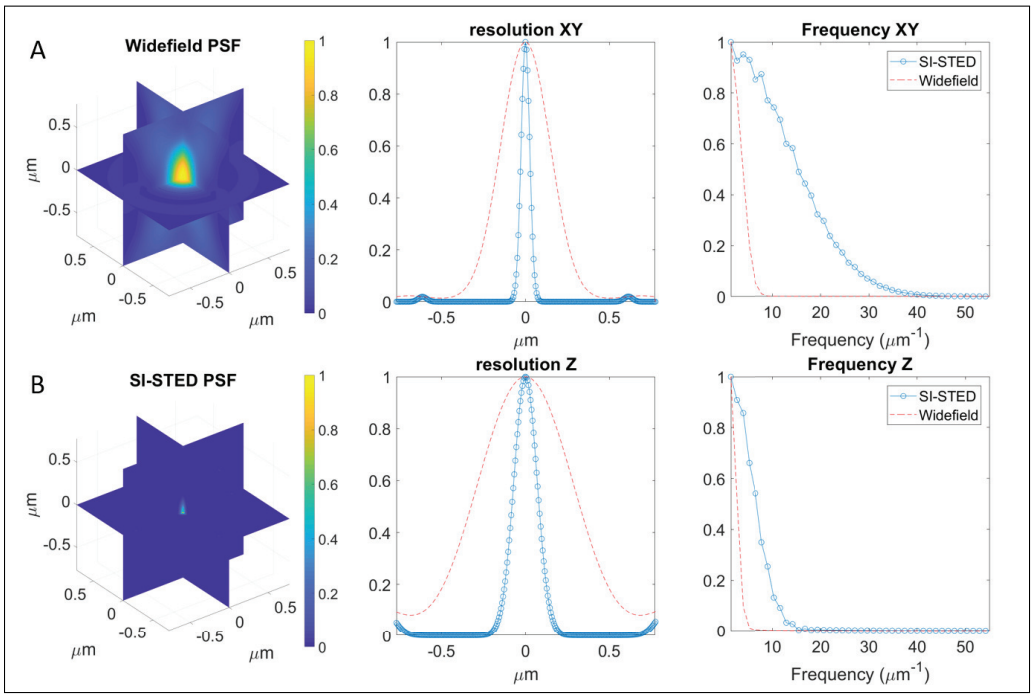

Fig. 5. The PSF comparison of (A) widefield microscopy and (B) SI-STED microscopy in 3D volume view. The cross-section comparison of (C) lateral PSF (D) axial PSF. The comparison of (E) lateral MTF and (F) axial MTF of widefield microscopy and SI-STED microscopy.

at 1 MHz repetition rate. Thus, the maximum number of dark nodes in one plane is 654 that corresponds to $12\mu m \times 12\mu m$ field of view.

As showed in Fig. 2, the SI generated by five beams coherent interference fills the "missing cone" in k_z of widefield microscopy. Next, we looked further into the 3D MTF of SI-STED microscopy. Point-scanning STED microscopy fills the "missing cone" based on confocal technique, so the axial resolution is the same of regular confocal microscopy. For SI-STED microscopy, the axial sectioning ability is from the 3D interferometric pattern (Fig. 2). We compared the 3D MTF of widefield and SI-STED microscopy (Fig. 6). SI-STED MTF is broadened than widefield MTF in both k_z and k_x direction. Thus, SI-STED microscopy not only has axial sectioning ability but also has better axial resolution than point scanning STED microscopy.

As we discussed in Section 2.3, the number of intermediate images for reconstruction relate to both pattern period and intensity. After the simulation, we can calculate the scanning speed according to the results in Fig. 4(b) and Fig. 5. The scanning within a plane is along the diagonal direction of the array because of the dark center positions. The SI pattern period is 473.9 nm in lateral direction and 661.6 nm in axial direction. The PSF of SI-STED microscopy is 59.9 nm in lateral direction and 163.2 nm in axial direction. According to Nyquist theorem, the minimum number of total steps to scan a 3D volume are $(473.9/59.9 \times 2)^2 \times (661.6/163.2 \times 2)^2 \approx 2030$. Assuming dwell time of STED in each scanning step is about 100 μs [9], the imaging speed of the volume is about $10\mu s \times 2030 = 203ms$. Thus, the SI-STED microscopy theoretically can reach 3D super-resolution at 5 Hz volume rate.

Optics EXPRESS

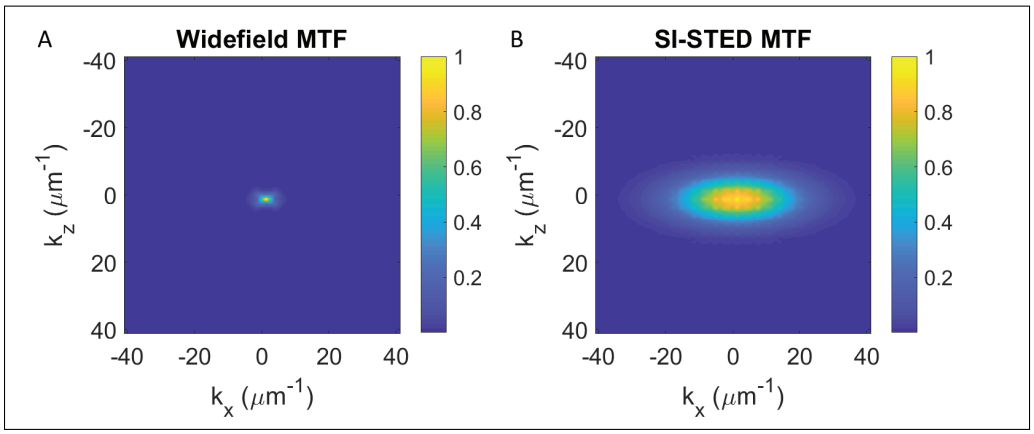

Fig. 6. The MTF of (A) widefield microscopy and (B) SI-STED microscopy in $k_x - k_z$ plane. Each figure is normalized to its peak value. Noticed the MTF of SI-STED microscopy is broadened in k_z, which fills the "missing cone" and has axial sectioning ability.

4. Conclusion

We demonstrate the design of SI-STED microscopy that achieves 3D high-throughput super-resolution imaging. The 3D SI-STED depletion pattern generated by five beams interference costs the same laser power as the 2D parallel STED microscopy, but the axial resolution is improved seven times breaking the diffraction limit. The technique is sensitive to polarization of the beam. Circular polarized beam can generate symmetric depletion patterns. The reason for axial section ability is filling the "missing-cone" of the frequency domain by structured illumination, and the nonlinear depletion process of STED microscopy further broadens the MTF. Thus, SI-STED microscopy can achieve 3D super-resolution. At the same time, SI depletion beam of STED microscopy improves the imaging speed by parallelization. It can reach 5 Hz volumetric imaging rate in theory. SI-STED microscopy potentially can be used for large volume super-resolution imaging of biological samples.

Funding

National Institutes of Health, USA (NIH 1-U01-NS090438-01, NIH 5-P41-EB015871).

Acknowledgement

The authors acknowledge support from Hamamatsu Corporation.